JOURNAL OF APPLIED CRYSTALLOGRAPHY
ISSN 1600-5767

Twinning and homoepitaxy cooperation in the already rich growth morphology of $CaCO_3$ polymorphs. I. Aragonite

Dino Aquilano,[a] Marco Bruno,[a,b]* Stefano Ghignone[a] and Linda Pastero[a,b]

[a]Dipartimento di Scienze della Terra, Università degli Studi di Torino, Via Valperga Caluso 35, 10125 Torino (TO), Italy, and [b]NIS, Centre for Nanostructured Interfaces and Surfaces, Università degli Studi di Torino, Via G. Quarello 15/a, 10135 Torino (TO), Italy. *Correspondence e-mail: marco.bruno@unito.it

Received 12 June 2023
Accepted 18 September 2023

Edited by J. M. García-Ruiz, Instituto Andaluz de Ciencias de la Tierra, Granada, Spain

Keywords: aragonite; twinning; homo-epitaxy; growth morphology.

Supporting information: this article has supporting information at journals.iucr.org/j

Calcite and aragonite are the two most abundant among the $CaCO_3$ polymorphs and are also well known for their rich morphology and habit, to which twinning relevantly contributes. Moreover, the calcite → aragonite transformation has been debated for a long time, even though the homo-epitaxies occurring within each polymorph have been overlooked, to date, from both experimental and theoretical points of view. Twinning is common and unfortunately can be deceptive as it can be mistaken for homo-epitaxy, thus leading to confusion regarding the growth mechanisms of many crystal aggregates. Here, experimental and theoretical studies were carried out to investigate the twinning and homo-epitaxy that operate in aragonite: (i) the connection between twinning and homo-epitaxy for contact and penetration aggregates made by the lateral {010} and {110} aragonite forms; (ii) the homo-epitaxial relationships among the {001} pinacoid and both the {010} pinacoid and the prismatic {110} aragonite forms. This work attempts to provide a new approach to monitoring the growth mechanisms of aragonite in cases where it is obtained not as a single crystal but as an aggregate. An analogous problem will be explored in our forthcoming work on calcite.

1. Introduction

1.1. Deviations from single-crystal morphology: historical aspects

To introduce the crystallographic novelty of the present work, we recollect some definitions which were given many years ago during lectures (Kern, 1989, 1996) where fundamental papers about single-crystal morphology deviations were reviewed (Friedel, 1926; Royer, 1928; Bailey *et al.*, 1977). It is unsurprising that 25 years ago the term 'homo-epitaxy' was often confused with the all-encompassing term 'epitaxy' (Kern, 1996). For this reason and out of respect for the past, it is necessary first to make these distinctions.

(i) Twinning concerns only one crystal species (A) and may occur during transitions or chemical reactions producing a crystal from other phases (vapour, solution, melt). Mechanical stresses can also be used to obtain twins from a pre-existing crystal phase. Hence, one can consider a twin to be like an anomaly or a defect with respect to a single homogeneous crystal, and two twinned individuals are related by a symmetry element that does not belong to the symmetry of crystal A.

(ii) Epitaxy occurs when a crystal A (deposit) is formed over another crystal B (substrate).

(iii) Endotaxy represents a more complex situation, in which a crystal A (exsolution) precipitates within a solid solution B (matrix) and the resulting aggregate is a composite.

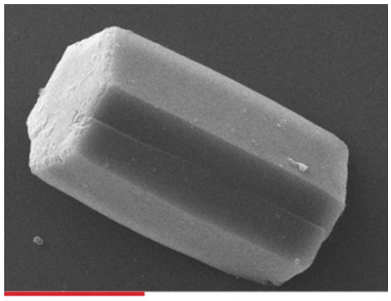

(iv) Topotaxy means that a crystal A is transformed (even incompletely) into another crystal B (chemically, thermally *etc.*). The conversion of a single crystal to one or more products will result in a crystal that has a definite crystallographic orientation with respect to the original, with the added requirements that the conversion occurs throughout the entire crystal and that there is a three-dimensional relationship between the initial and final structures. Accordingly, the resulting aggregation gives rise to pseudomorphism.

1.2. Why aragonite aggregates require homo-epitaxy

The term 'homo-epitaxy' will be used herein. Within the same crystal species (A), two or more different forms $\{hkl\}$ and $\{h'k'l'\}$ can associate in an epi-relation without producing a new twin law. Hence, we must be very careful when searching for the relationship between two $\{hkl\}$ forms of the same substance A and always check if there is any original composition plane (OCP) or a symmetry axis (which does not belong to the crystal A symmetry) intervening between the aforementioned forms.

Here, the aragonite (Arg herein, space group *Pnma*) homo-epitaxies $(010)_{Arg}/(110)_{Arg}$, $(001)_{Arg}/(010)_{Arg}$ and $(001)_{Arg}/(110)_{Arg}$ are studied at the empirical level; then we demonstrate that the pinacoidal $\{010\}_{Arg}$ form is homo-epitaxially related to the prismatic {110} form. Moreover, both $\{010\}_{Arg}$ and $\{110\}_{Arg}$ are also homo-epi-related with the basic $\{001\}_{Arg}$. Note that the {010} form coincides with the symmetry plane of aragonite and hence it cannot be a twin OCP, whereas the {110} faces are the historical OCPs of the well known aragonite twin (Massaro *et al.*, 2014).

We emphasize once again that we must clearly distinguish the homo-epitaxy (A/A → homo-epi) from both twinning (A/A → twins) and hetero-epitaxy (A/B → hetero-epi). Homo-epitaxy differs from the other two in both the geometric–reticular relationship and the role exerted by the crystal growth; we aim at determining whether the specific adhesion energy of the facing crystal forms plays an essential role in the crystal growth.

Also note that the calculated and relaxed equilibrium shape (ES) and the observed growth shape (GS) of aragonite will not be distinct here. The presence of small amounts of lithium in the mother growth solutions will reduce both ES and GS to the dominating {110}, {010} and {001} aragonite forms, as we have recently demonstrated (Aquilano *et al.*, 2019).

Finally, we outline the historical forgetfulness regarding the $\{010\}_{Arg}$ form, deemed essential especially in biological mineralization, where the shape of the flat $\{001\}_{Arg}$ pseudo-hexagonal tiles evidences the strategic role of $\{010\}_{Arg}$ in the shells of living organisms (Bruno *et al.*, 2022).

2. Computational method

To study the homo-epitaxial relationships in aragonite, we investigated the aforementioned epi-interfaces at the empirical level, determining both the structure and the thermodynamic properties at 0 K, and details of the computational methodology adopted for the interfaces are reported (Bruno *et al.*, 2015).

Accordingly, a composed slab of $(hkl)_{Arg}/(h'k'l')_{Arg}$ was generated (Bruno *et al.*, 2015, 2017): (i) we searched for the two-dimensional coincidence lattices (2D-LCs) between the (hkl) and $(h'k'l')$ faces of the Arg phase epi-related at the reticular level (discussed in the following paragraphs), and successively we considered only those fulfilling the rigorous epitaxy constraints (Table 1); (ii) $(hkl)_{Arg}$ and $(h'k'l')_{Arg}$ slabs of a selected thickness were made by cutting the bulk structure of the Arg phase parallel to the lattice planes of interest and using the same 2D-LC parameters describing the epitaxy; (iii) the $(hkl)_{Arg}$ slab was placed above the $(h'k'l')_{Arg}$ slab; (iv) finally, the composed slab structures (atomic coordinates and 2D-LC parameters) were optimized by considering that all the atoms are free to move.

Structure optimization of the $(010)_{Arg}/(110)_{Arg}$, $(001)_{Arg}/(010)_{Arg}$ and $(001)_{Arg}/(110)_{Arg}$ composed slabs was empirically performed using the calcium carbonate minerals force field (Rohl *et al.*, 2003) and version 4.0 of the *GULP* (*General Utility Lattice Program*) simulation code (Gale, 1997). The computational parameters that we adopted are suitable to guarantee convergence on the energy values discussed in the main text, as well as the thickness of the composed slabs. *GULP* output files with the optimized fractional coordinates and optimized 2D-LC parameters of the composed slabs are freely available at https://marco-bruno.weebly.com/download.html. We only performed static calculations at 0 K; the vibrational entropy and energy were not calculated. However, as we previously discussed (Bruno *et al.*, 2013; Bruno, 2015), neglecting the vibrational contribution should not lead to a significant error in the estimate of the adhesion and interfacial energies. The specific adhesion energy (erg cm^{-2}) is given by

$$\beta_{Arg}^{(hkl)/(h'k'l')} = \frac{E_{(h'k'l')}^{Arg} + E_{(hkl)}^{Arg} - E_{(hkl)/(h'k'l')}^{Arg/Arg}}{S}, \qquad (1)$$

where $E_{(hkl)/(h'k'l')}^{Arg/Arg}$, $E_{(h'k'l')}^{Arg}$ and $E_{(hkl)}^{Arg}$ represent the energies of the $(hkl)_{Arg}/(h'k'l')_{Arg}$ composed slab and the isolated $(h'k'l')_{Arg}$ and $(hkl)_{Arg}$ slabs, respectively, and S is the 2D-LC area. The value $\beta_{Arg}^{(hkl)/(h'k'l')}$ is closely related to the interface energy $\gamma_{Arg}^{(hkl)/(h'k'l')}$ (erg cm^{-2}) by the Dupré relation:

$$\gamma_{Arg}^{(hkl)/(h'k'l')} = \gamma_{Arg}^{(hkl)} + \gamma_{Arg}^{(h'k'l')} - \beta_{Arg}^{(hkl)/(h'k'l')}, \qquad (2)$$

where $\gamma_{Arg}^{(hkl)}$ and $\gamma_{Arg}^{(h'k'l')}$ are the specific surface energies under vacuum of the (hkl) and $(h'k'l')$ faces of the Arg phase, respectively.

Concerning Table 1, the maximum values of the percentage linear and area misfits (between the 2D-LC cells of the host and guest lattices) are determined by the difference of the cell vectors divided by the lowest of the two values. For instance, for the first example shown in Table 1, the linear misfit is calculated as (9.9222 − 9.3859)/9.3859 = +5.71%. The corresponding area misfit is (56.9604 − 53.8816)/53.8816 = +5.71%. The three best out of the five 2D supercells are rectangular, which means that their obliquity is null.

Table 1
2D-LCs between {110}//{010}, {110}//{001} and {010}//{001} couplings of aragonite.

2D-LCs with rank (1) are the best for calculating the adhesion energy in the related homo-epitaxy.

	Rank	$\{110\}_{Arg}$	$\{010\}_{Arg}$	Linear and area misfit (%)	Notes
2D-cell vectors (Å)	(1)	$[00\bar{1}] = 5.7407$	$[001] = 5.7407$	0	Rectangular
		$[1\bar{1}0] = 9.3859$	$2[100] = 9.9222$	+5.71	2D-supercell
2D-cell area (Å^2) and multiplicity		53.8816 (1×)	56.9604 (2×)	+5.71	

	Rank	$\{110\}_{Arg}$	$\{001\}_{Arg}$	Linear and area misfit (%)	Notes
2D-cell vectors (Å)	(1)	$3[00\bar{1}] = 17.2221$	$2[010] = 15.9354$	−8.07	Rectangular
		$[1\bar{1}0] = 9.3859$	$2[100] = 9.9222$	+5.71	2D-supercell
2D-cell area (Å^2) and multiplicity		161.6449 (3×)	158.114 (4×)	−2.23	
2D-cell vectors (Å)	(2)	$4[00\bar{1}] = 22.9628$	$3[010] = 23.9031$	+4.09	
		$[1\bar{1}0] = 9.3859$	$2[100] = 9.9222$	+5.71	
2D-cell area (Å^2) and multiplicity		215.5265 (4×)	237.171 (6×)	+10.04	

	Rank	$\{010\}_{Arg}$	$\{001\}_{Arg}$	Linear and area misfit (%)	Notes
2D-cell vectors (Å)	(1)	$3[001] = 17.2221$	$2[010] = 15.9354$	−8.07	Rectangular
		$[100] = 4.9611$	$[100] = 4.9611$	+0.00	2D-supercell
2D-cell area (Å^2) and multiplicity		85.4405 (3×)	79.0571 (2×)	−8.07	
2D-cell vectors (Å)	(2)	$7[001] = 40.1849$	$5[010] = 39.8385$	−0.87	
		$[100] = 4.9611$	$[100] = 4.9611$	+0.00	
2D-cell area (Å^2) and multiplicity		199.361 (7×)	197.642 (5×)	−0.87	

Table 2
Ca concentration, solution volume and Li^{1+}/Ca^{2+} mole ratios adopted in the Li^{1+}-doped growth experiments.

Concentration of Ca^{2+} in solution (moles)	Volume (ml)	Li^{1+}/Ca^{2+} (mole ratio)
5×10^{-3}	50	50
5×10^{-3}	50	70
5×10^{-3}	50	100
5×10^{-3}	50	150
5×10^{-3}	50	200

3. Experimental details

First, $CaCO_3$ solutions (5 m*M* in Ca^{2+}) were obtained by dissolving $CaCO_3$ (reagent grade, Sigma–Aldrich) in ultrapure (18 MΩ) water by bubbling CO_2 until a clear solution was obtained at room temperature and pressure. Solutions were filtered through qualitative filter papers to avoid calcium carbonate particles in suspension acting as nucleation centres for precipitating crystals. The Ca concentration was checked using a Thermo Jarrell Ash Corp. inductively coupled plasma optical emission spectrometer calibrated at 1 and 10 p.p.m. on a multi-element standard (Sigma–Aldrich).

Secondly, calcium carbonate solutions divided into 50 ml aliquots were placed in crystallizers. At the beginning, pure aqueous solutions were used (not quoted in Table 2), while Li^+ ions were added as LiCl at different concentrations to each crystallizer to evaluate the effect of the Li^+/Ca^{2+} ratio on both the polymorphs and the morphology selection (Table 2). To identify outliers, each experiment was carried out three times.

The dissolved carbonate was left to equilibrate with the atmospheric CO_2. Crystals nucleated onto clean glass slides, vertically placed at the bottom of the vessels to ensure only the *in situ* newly formed crystals were collected at the end of the experiments. The crystals grown on the glass slides were gently washed with deionized water to avoid secondary nucleation and decoration of the surface features and left to dry at room temperature overnight. Imaging was performed using a Cambridge S-360 scanning electron microscope (SEM) (EHT 30 kV, working distance 5 mm, current probe 100 pA).

4. Acquired results, in-house experiments and discussion

4.1. Selected twinning and homo-epitaxies between the {110}, {010} and {001} forms of aragonite

The specific twin energy γ_{TE}^{hkl} (erg cm^{-2}) is the energy to be spent on a given (*hkl*) face in order to form a twin on it. The aragonite structure and morphology have been studied for a long time (Goldschmidt, 1913; Massaro *et al.*, 2014) and we recall that the sole {110} twin law reads $\gamma_{TE}^{(110)} = 17$ erg cm^{-2}.

Returning to the (A/B) epitaxy, it seems natural to assume that the epitaxy between two crystal structures (calcite = Cal and aragonite = Arg) should be more expensive than twinning or homo-epitaxy. Actually, this is true for the $(01.2)^{Ca}_{Cal}/(010)^{Ca}_{Arg}$ and $(10.0)_{Cal}/(110)^{Ca}_{Arg}$ epitaxies, which show interfacial epi-energies of 1551 and 1321 erg cm^{-2}, respectively (Bruno *et al.*, 2022). But this trend fails when considering that $\gamma^{(11.0)_{Cal}/(100)_{Arg}} = 713$ erg cm^{-2} and $\gamma^{(00.1)^{CO_3}_{Cal}/(001)^{CO_3}_{Arg}} = 294$ erg cm^{-2} (Bruno *et al.*, 2008, 2022).

In the $(11.0)_{Cal}/(100)_{Arg}$ epitaxy, and when the [001] direction is shared by the two crystals, the order of magnitude of the epitaxial energy is close to that of the homo-epitaxy; moreover, the two structures of calcite and aragonite can

compenetrate each other by sharing their carbonate lamellae which have perfectly parallel CO_3^{2-} groups with the elementary thicknesses d_{002}^{Arg} = 2.8703 Å and d_{006}^{Cal} = 2.8433 Å (with the related Δ% = 0.95). In the $(00.1)_{Cal}^{CO_3}/(001)_{Arg}^{CO_3}$ epitaxy, the interfacial energy is so low that thin 3D nuclei can form at the interface (Stranski & Krastanov, 1938), even at low-supersaturation values. Moreover, we showed that this epitaxy can evolve, even at room temperature, into a new polymorph with an intermediate symmetry (hexaragonite) between aragonite and calcite (Bruno *et al.*, 2022).

4.2. Reviewing the twinning in the [001] zone of aragonite: the {110} and {010} forms

As mentioned in the *Introduction* and illustrated in Fig. 1, single aragonite crystals and their classic {110} twin law have been known for some time (Goldschmidt, 1913; Bragg, 1924). For the present work, aragonite crystals have been grown in our laboratory where [001] prismatic-elongated mono-crystals, along with double and triple individuals, have been obtained (Fig. 2). Contrary to their equilibrium shape, the well developed {001} forms on their GSs clearly indicated both the penetration and the probable spiral origin of the entire twinned aggregates.

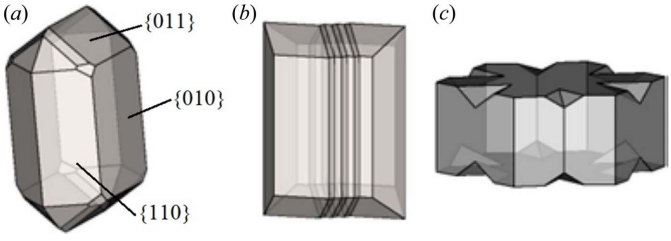

Figure 1
We examined (Aquilano *et al.*, 2019) the indexing of dominant forms belonging to more than 200 single and twinned aragonite crystals grown in different geological sites: (*a*) prismatic {110}, {011} and pinacoidal {010} forms on single crystals; (*b*) repeated contact {110} twins; (*c*) repeated penetration {110} twin showing the {001} form as well. Note that, from our historical research, the basal {001} form appears in 45% of twins and in only 23% of single crystals. Crystals redrawn after Goldschmidt (1913).

Moreover, the twin problem took a big step forward when both contact and penetration {110} twin laws were carefully examined in inorganic geological samples (Otálora *et al.*, 2018). These authors found (i) recurrent and protruding spurs between non-twinned individuals in the triple contact twins; and (ii) concavities in two opposite forms in the penetration twins. This novelty should be quite encouraging, but it remains unexplained why there is a sharp angular difference (∼11.50°) when the three twinned individuals are closing [Fig. 3(*a*)].

Otálora *et al.* (2018) studied the geological aragonite in its {001} natural thin sections, determining both angular concavities and spurs. At the same time, Aquilano *et al.* (2019) examined the effect of Li_2CO_3 *ad*-absorption on the growth morphology of in-house-made aragonite. Both studies focused their attention on the 'real development' of the $[001]_{Arg}$ growth zone and on the reciprocal influence between the {110} and {010} aragonite faces.

Although the importance of aragonite along with a comparison between Figs. 2 and 3 allowed us to address an age-old crystallographic and mineralogical problem from a broader perspective, we ask if, to date, adequate attention has been paid to the similarities and differences between the prismatic {110} and pinacoidal {010} forms of aragonite. Our question arises from the fact that surface dipoles, mainly attributed to CO_3^{2-} ions, should behave differently at the borders of d_{110} and d_{020} slices, but this does not affect the long-range properties, *e.g.* the surface and attachment energies; instead, short-range characteristics, such as solvent and impurity adsorption, may vary considerably from {110} to {010} forms, owing to the different orientation of dipole moments with respect to their surfaces.

Furthermore, it is rather strange that, in the drawings in the literature and in the above-mentioned article (Otálora *et al.*, 2018), the {010} form of aragonite has never been sufficiently considered. Owing to the aragonite space group, this strategic {010} pinacoid cannot work as a twin plane, but actively participates in both the ES and the GS of the crystal, as

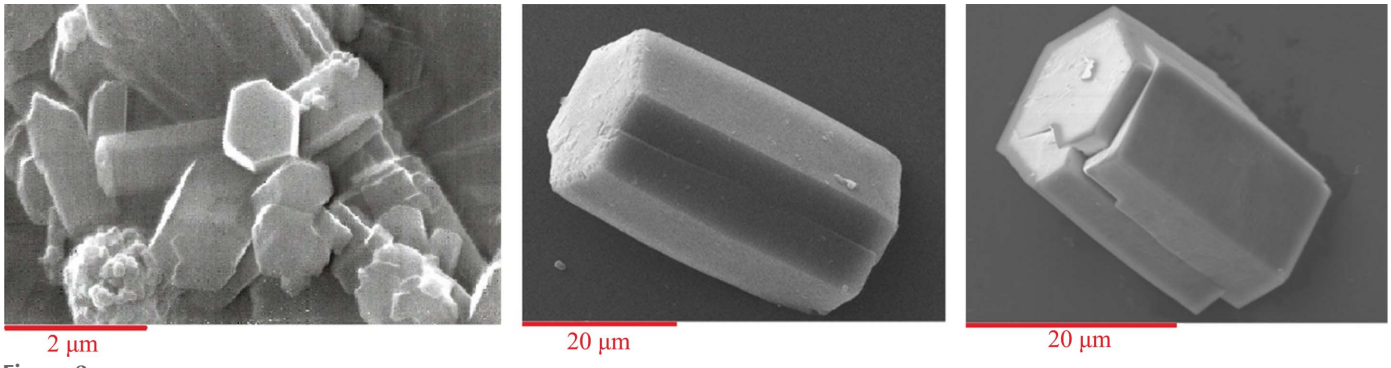

Figure 2
All aragonite crystals shown here were produced in-house. When grown from pure aqueous solutions (left), the pure {001} basic and pseudo-hexagonal pinacoidal forms do not show any re-entrant or salient angles. Otherwise, in the presence of lithium (see Table 2) the {001} pinacoids show welding between individuals composing the aggregates (centre and right). The complex twin (right) probably indicates the spiral origin of the fully closed aggregate [see also Aquilano *et al.* (2019)]. In the last two cases, it is impossible to distinguish between twinned and homo-epitaxial contributions, along with the {110} and {010} indexing of prismatic faces, since the measurement of the angles is not feasible in the SEM images.

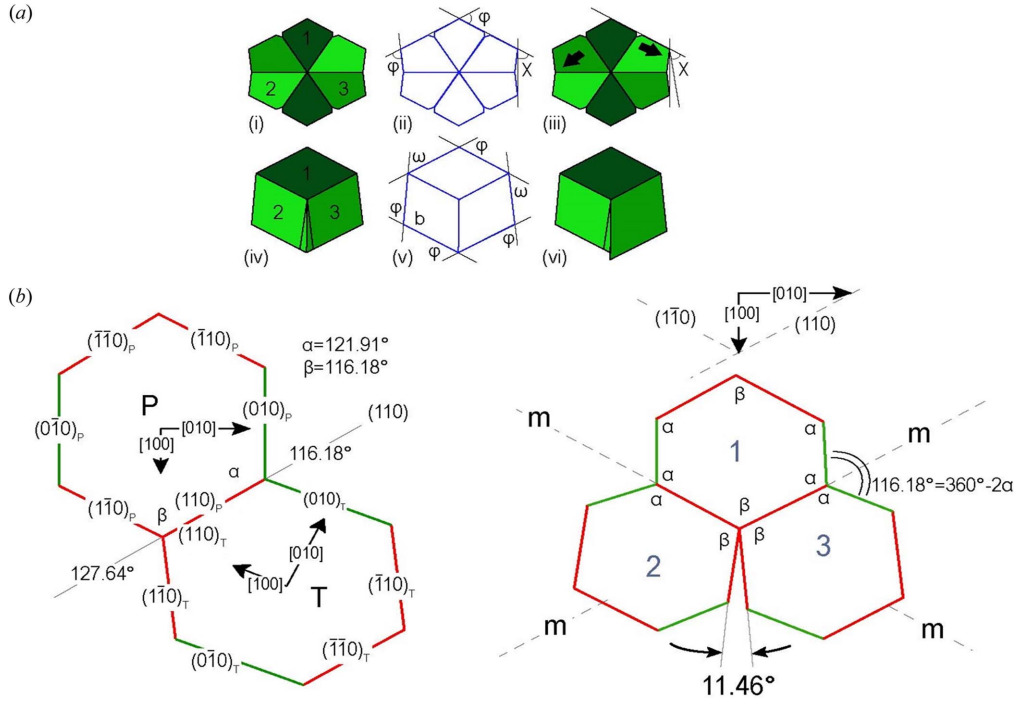

Figure 3
[001] projection of the twinned aragonite morphology. (*a*) Penetration (i), (ii), (iii) and contact (iv), (v), (vi) {110} twins of aragonite. Angles $\varphi = 63.824°$, $\chi = 58.088°$, $\omega = 52.352°$ [redrawn from Otálora *et al.* (2018)]. (*b*) Our elaboration of (*a*): parent (P and 1) and both twinned individuals (T and 2, 3) along with the $m \equiv \langle 110 \rangle$ twin planes; the indexes of the faces and the angles (α, β) they form are also indicated. Note: all the twin planes are parallel to the {110} faces; and individuals 1 and 2, along with 1 and 3, are twinned, whereas 2 and 3 are not twinned with each other, and hence there is no contact between their {110} faces (individuals 2 and 3).

commonly observed in inorganic and bio-mineralogical samples. In this regard, Checa *et al.* (2013) observed that the growth sectors associated with the $\{010\}_{Arg}$ form are vital in the formation of flat {001} nacre tablets.

Fig. 3 outlines the angular difference in a pure contact {110} twin of aragonite. The angle formed by $(010)_P$ and $(010)_T$ individuals (P = parent, T = twinned) should be 116.18°, whereas the opposite one, formed by $(1\bar{1}0)_P$ and $(1\bar{1}0)_T$ is 127.64° [Fig. 3(*b*), left]. Hence, a twin closure cannot exist [Fig. 3(*b*), right], the difference being $360° - 3\beta = (127.64 - 116.18°) = 11.46°$, as a consequence of the aragonite pseudo-hexagonality.

4.3. The cooperation between {110} twinning and homo-epitaxy in the [001] zone of aragonite

As anticipated in Section 4.1, the criticisms on the sole $\{110\}_{Arg}$ twinning arose from our hypothesis that both twinning and homo-epitaxy can cooperate in enriching the morphology of aragonite aggregates. Now the phenomenon of pure twinning has been considered, we want to address the coexistence between twinning and homo-epitaxy. Finally, we will examine the case in which the aragonite aggregate is formed in the [001] zone owing to the pure homo-epitaxy.

First, we consider the consequences of homo-epitaxy onto a classic aragonite single crystal: how will the bi-crystal be made?

In Figs. 4(*a*) and 4(*b*), the parent crystal is the same as the quoted example, whereas the generated one is not twinned, but obtained through simple homo-epitaxy (H) in which a pinacoidal {010} face adheres to a prismatic {110} parent one through a simple geometric rotation. Accordingly, one can replace twinning with homo-epitaxy and the substitution would not be noticeable, since the as-built bi-crystal is morphologically identical to the twinned one. A difference of course exists, but only for their surfaces: in fact, the surface {010} patterns (either growth or corrosion) should markedly differ from the {110} ones.

We can now assume that twinning and homo-epitaxy could coexist, as in Fig. 4(*c*): a bi-crystal ($P\text{-}T_{110}$) is twin-generated and a triple crystal is made since a new individual is added by homo-epitaxy from P to H2 ($P\text{-}T_{110}\text{-}H2$). It can be easily ensured that not only is the aragonite pseudohexagonality preserved but the absolute angular misfit is halved ($\Delta = 5.73°$ being equal to $121.91 - 116.18°$) with respect to that obtained when pure twinning has been considered.

Finally, we now imagine the triple-crystal aggregate as originated from pure homo-epitaxy. In Fig. 4(*d*), the H1 and H2 individuals have been added through rotations around [001] in such a way that two successive homo-epitaxies form the aggregate. Dashed lines represent the contact planes. The novelty is now apparent: the closure is complete and perfect and the final aggregate has been built by homo-epitaxies only. By allowing the crystal set to grow, all the re-entrant angles disappear, the final result reproducing exactly the angles ($2\beta + 4\alpha$) and the shape of the original parent crystal (external dashed lines).

Returning to the case of twinning and homo-epitaxy cooperation [Fig. 4(*c*)], one can see that here the growing

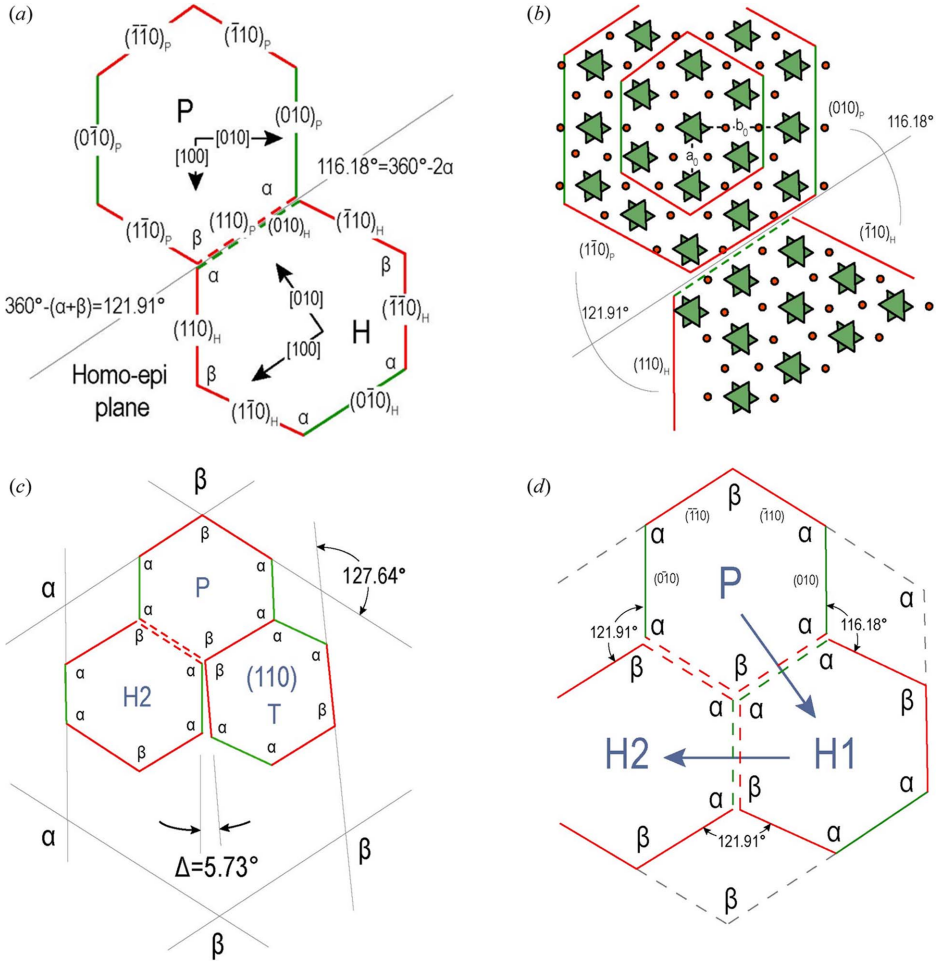

Figure 4
(*a*) The parent crystal (left) generates a second one which is not twinned: it is obtained by homo-epitaxy in which a pinacoidal {010} face adheres to a parent prismatic {110} one. (*b*) A detailed version of the drawing in (*a*); both carbonate and calcium ions are represented in such a way that the continuity between parent (P) and homo-epitaxy (H) structures is emphasized. (*c*) From the parent crystal both a twinned (T) (110) and a homo-epitaxy individual (H2) are generated. (*d*) Another equivalent (H1) is made, always by the same homo-epitaxy law. Hence a triple aggregate has been obtained by homo-epitaxy only.

triple aggregate does not reproduce the angles of the P crystal; in fact, the internal angles $(3\beta + 2\alpha) + 127.64^\circ$ are no longer symmetric as a consequence of the cooperation.

4.4. The homo-epitaxy between the {110} and {010} forms of aragonite

The 2D-LCs between these two lateral forms (Table 1) are very simple. Our calculations were carried out by considering the $(010)_{Ca}/(110)_{Ca}$, $(010)_{CO_3}/(110)_{Ca}$ and $(010)_{Ca}/(110)_{CO_3}$ interfaces. The associated adhesion energies are $\beta_{Arg}^{(010)_{Ca}/(110)_{Ca}} = 752$ erg cm^{-2}, $\beta_{Arg}^{(010)_{CO_3}/(110)_{Ca}} = 395$ erg cm^{-2} and $\beta_{Arg}^{(010)_{Ca}/(110)_{CO_3}} = -538$ erg cm^{-2}. Using equation (1), the Dupré relation (Kern, 1978) and the surface energy values already calculated by Massaro *et al.* (2014) ($\gamma_{Arg}^{(010)_{Ca}} = 808$ erg cm^{-2}, $\gamma_{Arg}^{(010)_{CO_3}} = 1199$ erg cm^{-2}, $\gamma_{Arg}^{(110)_{Ca}} = 730$ erg cm^{-2}, $\gamma_{Arg}^{(110)_{CO_3}} = 1051$ erg cm^{-2}), the interface energies are found to be $\gamma_{Arg}^{(010)_{Ca}/(110)_{Ca}} = 786$ erg cm^{-2}, $\gamma_{Arg}^{(010)_{CO_3}/(110)_{Ca}} = 1534$ erg cm^{-2} and $\gamma_{Arg}^{(010)_{Ca}/(110)_{CO_3}} = 2397$ erg cm^{-2}. Accordingly, the most stable interface is $(010)_{Ca}/(110)_{Ca}$. This agrees with the evidence that the slices

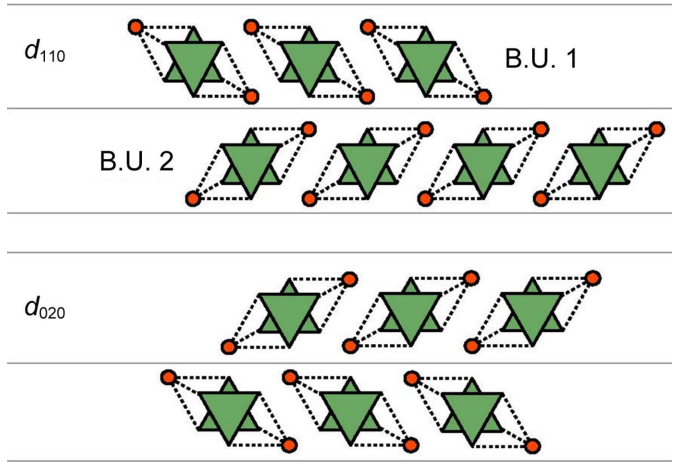

Figure 5
Structure of the slices d_{110}^{Arg} and d_{020}^{Arg}, both belonging to the [001] zone of aragonite: the {110} prism can show two profiles that are pseudo-symmetrically equivalent, generated from two types of building units (BU_1 or BU_2), whereas the {010} pinacoid, whose profile should be unique, is built by BU_2 only. Note the strong similarity between the d_{020}^{Arg} and d_{110}^{Arg} slices. The meaning of the term 'building unit' has been described previously elsewhere (Aquilano *et al.*, 1997) and the bonds that make each BU are illustrated in detail.

of thickness d_{110}^{Arg} and d_{020}^{Arg} (Fig. 5), which are always Ca-terminated, were defined as self-consistent (Hartman & Perdok, 1955; Aquilano *et al.*, 1997).

4.5. The homo-epitaxy of the basic {001} pinacoid with the prismatic {110} and {010} pinacoidal forms of aragonite: its peculiar pseudo-hexagonality

It is not trivial taking advantage of the facts to outline once more the peculiar pseudo-hexagonality of aragonite. Many others have remarked on this feature by looking at aragonite along its [001] direction: it is obviously true, when recollecting that a pseudo-hexagonal {001} supercell is obtained (multiplicity = 6×) with an area of 237.17 Å^2, along with two angles of 116.18° between the ⟨110⟩ directions, and 121.91° between the ⟨110⟩ and the [100] directions (Fig. 6, right). But it is easy to understand why one can pass from the $\{110\}_{Arg}$ to the $\{010\}_{Arg}$ form simply through homo-epitaxy (Fig. 6, left and centre). Hence, Fig. 6 allows us to visualize the pseudo–hexagonality of the {001}, {110} and {010} aragonite cells.

Once this has been established, we should not be surprised if the $\{001\}_{Arg}$ form faces the lateral {010} and {110} ones, making a contact with them that cannot be twinning but only homo-epitaxy.

To test this, calculations have been made by considering the lattice compatibilities listed in Table 1 and the following interfaces: $(001)_{Ca}/(010)_{Ca}$, $(001)_{CO_3}/(010)_{Ca}$, $(001)_{Ca}/(110)_{Ca}$ and $(001)_{CO_3}/(110)_{Ca}$. The associated adhesion energies are $\beta_{Arg}^{(001)_{Ca}/(010)_{Ca}} = 1369$ erg cm^{-2}, $\beta_{Arg}^{(001)_{CO_3}/(010)_{Ca}} = 345$ erg cm^{-2}, $\beta_{Arg}^{(001)_{Ca}/(110)_{Ca}} = 1202$ erg cm^{-2} and $\beta_{Arg}^{(001)_{CO_3}/(110)_{Ca}} = -198$ erg cm^{-2}. Again, by employing the Dupré relation and the previously calculated surface energies ($\gamma_{Arg}^{(001)_{Ca}} = 1077$ erg cm^{-2}, $\gamma_{Arg}^{(001)_{CO_3}} = 779$ erg cm^{-2}, $\gamma_{Arg}^{(010)_{Ca}} = 808$ erg cm^{-2}, $\gamma_{Arg}^{(110)_{Ca}} = 730$ erg cm^{-2}), the interface energies are found to be $\gamma_{Arg}^{(001)_{Ca}/(010)_{Ca}} = 516$ erg cm^{-2}, $\gamma_{Arg}^{(001)_{CO_3}/(010)_{Ca}} = 1242$ erg cm^{-2}, $\gamma_{Arg}^{(001)_{Ca}/(110)_{Ca}} = 605$ erg cm^{-2} and $\gamma_{Arg}^{(001)_{CO_3}/(110)_{Ca}} = 1707$ erg cm^{-2}. Accordingly, the more stable interfaces are $(001)_{Ca}/(010)_{Ca}$ and $(001)_{Ca}/(110)_{Ca}$. This unambiguous result allows us to assert that only the Ca-terminated surfaces must be chosen for both d_{002}^{Arg} and d_{020}^{Arg} aragonite layers in order to obtain a homo-epitaxial contact between them.

What is really new is that, after the geometry optimization of the interfaces, the intermediate phase of hexaragonite (space group $P6_322$) cannot be forgotten (Bruno *et al.*, 2022). In fact:

(i) Hexaragonite is generated at the {001}/{110} interface, only when the facing forms are $(001)_{Ca}/(110)_{Ca}$.

(ii) Both {001} terminations turn into hexaragonite with the {010} form, but only if {010} is Ca-terminated.

4.6. Comparing the thickness of the d_{002} aragonite layers with d_{020} and d_{110} spacings: hypotheses on their growth mechanisms

The comparison between the stackings of the aragonite forms involved in the homo-epitaxies between the basal {001} and both the pinacoid {010} and the {110} prism highlights a non-negligible fact if we also want to look at the growth mechanisms intervening in this complex case. From Fig. 7 we can be certain that these are not random and non-periodic coincidences, which means that neither Volmer–Weber (Volmer & Weber, 1926) nor Stranski–Krastanow (Stranski & Krastanov, 1938) mechanisms can be easily assigned in our epitaxies. Rather, it is more effective to refer to another option (Frank & Merwe, 1949) where a good adhesion energy between the epi-partners is needed, as can be inferred from the calculations (2D-LCs and involved interfaces) shown in the present work.

5. Twinning and homo-epitaxies optically identified in aragonite aggregates

To establish whether a pseudo-hexagonal triple aragonite aggregate is the result of three individuals related by twinning

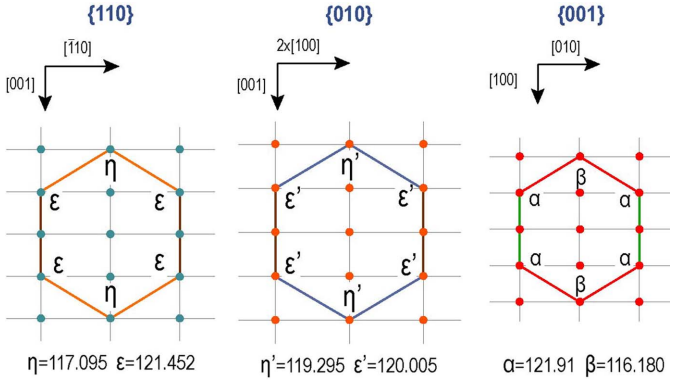

Figure 6
The pseudo-hexagonal 2D cells of aragonite (multiplicity = 6×) can be drawn for the prismatic {110} (left) and pinacoidal {010} (centre) forms, both parallel to its [001] zone. The pinacoidal {001} (right) form has also been added to allow comparison between these main forms. In the three drawings the scalar ratio is preserved.

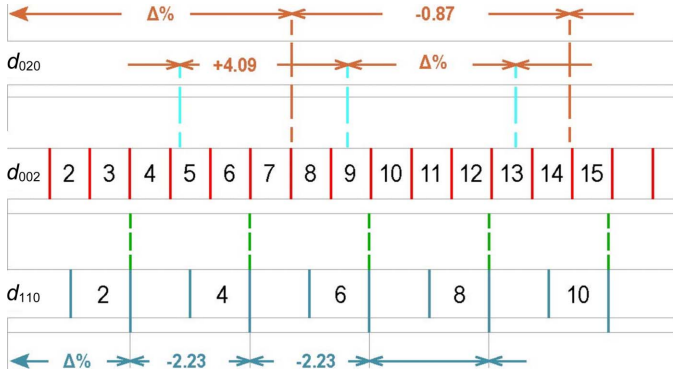

Figure 7
In aragonite, the thickness of the (001) planes fits very well with that of the (110) planes; in fact, one can verify that $\Delta\% = (3 \times d_{002}^{Arg} - 2 \times d_{110}^{Arg})\% = -2.23$, which is a very short range coincidence. The same does not occur when comparing the (001) thicknesses with those of (010). Instead, in this case one has two medium–long-range opportunities. In the first, $\Delta\% = (4 \times d_{002}^{Arg} - 3 \times d_{020}^{Arg})\% = +4.09$, whereas in the second a better percent coincidence is obtained, even though the related distances are wider: $\Delta\% = (7 \times d_{002}^{Arg} - 5 \times d_{020}^{Arg})\% = -0.87$.

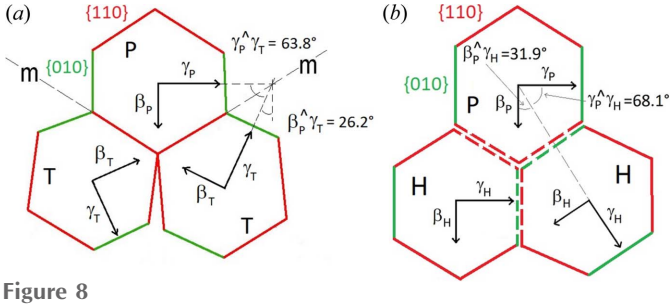

Figure 8
Extinction angles in triple aragonite aggregates related by (*a*) twinning and (*b*) homo-epitaxy. The aggregates are observed along [001]; $\alpha \equiv [001]$, $\beta \equiv [100]$ and $\gamma = [010]$ are the main refractive indexes of aragonite.

[Fig. 3(*b*)] or homo-epitaxy [Fig. 4(*d*)], we have to perform cross-polarizer optical observations on a thin section of the aragonite aggregate perpendicularly cut to the [001] direction (Fig. 8). Aragonite is a biaxial crystal with the optical indicatrix oriented in the following way: $\alpha \equiv [001]$, $\beta \equiv [100]$ and $\gamma \equiv [010]$ (Deer *et al.*, 1992), where α = 1.530–1.531, β = 1.680–1.681 and γ = 1.685–1.686 are the main refractive indexes of aragonite. Then, the extinction angles between twinned individuals [Fig. 8(*a*)] or in the homo-epitaxial relationship [Fig. 8(*b*)] will necessarily be different: $\beta_P^{\gamma_T} = 26.2^\circ$ and $\beta_P^{\gamma_H} = 31.9^\circ$.

6. Conclusions

Aragonite, one of the $CaCO_3$ polymorphs, has always shown recurrent production of twins, *i.e.* the celebrated {110} twin law. Moreover, we recently demonstrated that the aragonite → calcite transition can occur, through a new phase (hexaragonite), at ambient temperature and presure (Bruno *et al.*, 2022). Here, we demonstrated that there is a growth mechanism capable of generating a special kind of epitaxy within the same crystalline phase; hence, we called it homo-epitaxy. All these phenomena resemble each other, and the thermodynamic quantity that unites and distinguishes them is the specific adhesion energy between the facing crystal phases.

In aragonite, the {110} twin law is subject to ambiguity. However, the interface energies involved are all specific, *i.e.* they are expressed per unit area (erg cm^{-2}); this means that, in our evaluation, the crystal extension in the [001] zone is irrelevant. It seems reasonable to compare the production of (i) three single aragonite crystals, each independent; (ii) one double contact twin [Fig. 3(*b*)]; and (iii) one triple crystal obtained through homo-epitaxy only [Fig. 4(*d*)]. With these values, we evaluated the whole surface/interface energetic contribution of these numerically equivalent crystal sets:

(i) Three single crystals of aragonite with 3 × [2 × (010) + 4 × (110)] free faces

$$\rightarrow \gamma_{\text{Aggregate}} = 3 \times \left(2 \times \gamma_{\text{Arg}}^{(010)_{\text{Ca}}} + 4 \times \gamma_{\text{Arg}}^{(110)_{\text{Ca}}}\right) = 13608\ \text{erg cm}^{-2}.$$

(ii) One double contact twin [Fig. 3(*b*)] made by [6 × (010) + 8 × (110)] free faces + 2 × (110) twin interfaces

$$\rightarrow \gamma_{\text{Aggregate}} = \left(6 \times \gamma_{\text{Arg}}^{(010)_{\text{Ca}}} + 8 \times \gamma_{\text{Arg}}^{(110)_{\text{Ca}}}\right) + 2 \times \gamma_{\text{TE}}^{(110)} = 17022\ \text{erg cm}^{-2}.$$

(iii) One triple crystal obtained from homo-epitaxy only [Fig. 4(*d*)], made by [4 × (010) + 8 × (110)] free faces + 1 × (110) twin interface + 2 × (010)/(110) homo-interfaces

$$\rightarrow \gamma_{\text{Aggregate}} = \left(4 \times \gamma_{\text{Arg}}^{(010)_{\text{Ca}}} + 8 \times \gamma_{\text{Arg}}^{(110)_{\text{Ca}}}\right) + 1 \times \gamma_{\text{TE}}^{(110)} + 2 \times \gamma_{\text{Arg}}^{(010)_{\text{Ca}}/(110)_{\text{Ca}}} = 10661\ \text{erg cm}^{-2}.$$

Accordingly, it is plain that, in the [001] aragonite zone, the {*hk*0} forms related either by homo-epitaxy or by contact twinning are practically equivalent. This result is quite interesting because, to our knowledge, it is the first time that homo-epitaxy and contact twinning have the same probability of occurring. In any case, the production of single {*hk*0} crystals is morphologically less important than the production of crystals obtained either by homo-epitaxy or by twinning. Using the concept of morphological importance, one can make the assertion [{010}, {110}] single forms ≪ {010}/{110} homo-epitaxy ≃ {110} twins.

A completely different situation occurs if new homo-epitaxies are taken into account. That is, the {001} pinacoidal aragonite form establishes a crystallographic contact either with {010} pinacoidal or with {110} prismatic forms of aragonite itself; numerous cases of this eventuality are documented. In both cases it should be first remembered that the position of triangular carbonate groups in the {001} pinacoidal aragonite form is horizontal (*i.e.* perpendicular to the [001] aragonite direction), whereas in both {010} and {110} the CO_3^{2-} groups are parallel to [001] of aragonite: it is therefore a matter of bringing together two orthogonal carbonate positions in both cases. When such an event occurs, the following transformations ensue at room temperature and pressure:

(i) Hexaragonite ($P6_322$) is generated at the {001}/{110} interface, but only when both facing forms are Ca-terminated. Here, the new polymorph develops perpendicular to the {110} surface of aragonite.

(ii) Both {001} terminations turn into hexaragonite with the {010} form, but only if {010} is Ca-terminated. It follows that also in this case hexaragonite runs perpendicular to the {010} surface, irrespective of the {001} termination.

To summarize, having considered these results (Bruno *et al.*, 2022), it is plausible that aragonite crystals can turn into hexaragonite along the three main directions of aragonite: [001], [010] and [*uv*0], perpendicular to the {110} form.

For the reasons discussed here, and considering that the homo-epitaxy has been studied up to now as a peculiar case of opto-electronic devices, we suggest that the polymorphic calcite–aragonite system requires a closer re-examination, from both crystallography and crystal growth perspectives.

References

Aquilano, D., Pastero, L. & Bruno, M. (2019). *Cryst. Growth Des.* **19**, 3969–3978.

Aquilano, D., Rubbo, M., Catti, M. & Pavese, A. (1997). *J. Cryst. Growth*, **182**, 168–184.
Bailey, S. W., Frank-Kamenetskii, V. A., Goldsztaub, S., Kato, A., Pabst, A., Schulz, H., Taylor, H. F. W., Fleischer, M. & Wilson, A. J. C. (1977). *Acta Cryst.* A**33**, 681–684.
Bragg, W. L. (1924). *Proc. R. Soc. London A*, **105**, 16–39.
Bruno, M. (2015). *CrystEngComm*, **17**, 2204–2211.
Bruno, M., Massaro, F. R. & Prencipe, M. (2008). *Surf. Sci.* **602**, 2774–2782.
Bruno, M., Massaro, F. R. & Rubbo, M. (2017). *CrystEngComm*, **19**, 3939–3946.
Bruno, M. & Prencipe, M. (2013). *CrystEngComm*, **15**, 6736–6744.
Bruno, M., Prencipe, M., Aquilano, D., Cotellucci, A., Ghignone, S. & Németh, P. (2022). *J. Phys. Chem. C*, **126**, 6472–6481.
Bruno, M., Rubbo, M., Pastero, L., Massaro, F. R., Nestola, F. & Aquilano, D. (2015). *Cryst. Growth Des.* **15**, 2979–2987.
Checa, A. G., Mutvei, H., Osuna-Mascaró, A. J., Bonarski, J. T., Faryna, M., Berent, K., Pina, C. M., Rousseau, M. & Macías-Sánchez, E. (2013). *J. Struct. Biol.* **183**, 368–376.
Deer, W. A., Howie, R. A. & Zussman, J. (1992). Editors. *An Introduction to the Rock-Forming Minerals.* New York: Wiley.
Frank, F. C. & van der Merwe, J. H. (1949). *Proc. R. Soc. London A*, **198**, 205–216.
Friedel, G. (1926). *Leçons de Cristallographie.* Nancy, Paris, Strasbourg: Berger–Levrault.
Gale, J. D. (1997). *Faraday Trans.* **93**, 629–637.
Goldschmidt, V. (1913). Editor. *Atlas der Krystallformen*. Berlin: Winter.
Hartman, P. & Perdok, W. G. (1955). *Acta Cryst.* **8**, 49–52.
Kern, R. (1978). *Bull. Mineral.* **101**, 202–233.
Kern, R. (1989). *Crystal Growth in Science and Technology*, edited by H. Arend & J. Hulliger, pp. 143–165. New York: Plenum Press.
Kern, R. (1996). *A Short Course on Crystal Growth in Earth Sciences*, edited by E. Scandale & A. Baronnet, pp. 129–163. S. Vittoria d'Alba: Fecha de Publicación.
Massaro, F. R., Bruno, M. & Rubbo, M. (2014). *CrystEngComm*, **16**, 627–635.
Otálora, F., Mazurier, A., Garcia-Ruiz, J. M., Van Kranendonk, M. J., Kotopoulou, E., El Albani, A. & Garrido, C. J. (2018). *J. Appl. Cryst.* **51**, 1050–1058.
Rohl, A. L., Wright, K. & Gale, J. D. (2003). *Am. Mineral.* **88**, 921–925.
Royer, L. (1928). *Bull. Soc. Fr. Miner. Crist.* **51**, 7–159.
Stranski, I. N. & Krastanov, L. (1938). *Akad. Wiss. Wien*, **146**, 797–810.
Volmer, M. & Weber, A. (1926). *Z. Phys. Chem.* **119U**, 277–301.